# Corrosion Performance of Steel Rebars in the Roof of a 65-Year-Old Underground Reinforced Concrete Water-Storage Tank

Iman Taji[1]; Saeid Ghorbani[2]; Reza Johari Teymoori[3]; Mehrdad Hoseinpoor[4]; Ali Davoodi[5]; Arash Raouf Sheibani[6]; Mohammadreza Mohammadi[7]; and Jorge de Brito[8]

**Abstract:** This work deals with the corrosion evaluation of steel rebars in an underground water-storage tank using visual inspection, half-cell potential, and electrochemical impedance spectroscopy (EIS). The studied case has a service life of 65 years. From the inside, red stains were observed on the roof of the tank, and some cracks, as well as spalling of the concrete's cover, raised suspicion of corrosion damage. Twenty-seven points on the tank's roof were selected to drill out cores for further investigation. Measurements of the chloride penetration in the roof showed that the bottom part of the roof that was exposed to greater humidity and chloride-laden vapor was at risk of heavy corrosion. EIS studies of the steel rebars at different depths confirmed that those located in the upper part of the roof still have appropriate resistance to corrosion, but the lower ones exhibited a high corrosion rate. As a result, a repair of at least 12 cm in depth of the bottom of the roof and the installation of a proper ventilation system inside the tank were recommended. **DOI: 10.1061/(ASCE)CF.1943-5509.0001481.** 

**Author keywords:** Case study; Reinforced concrete underground water storage tank; Half-cell potential; Electrochemical impedance spectroscopy; Steel rebar corrosion.



## Introduction

Conventional RC storage tanks have been widely used in municipal and industrial facilities to store potable drinking water, wastewater, and rainwater for many decades. There are three different types of water tanks: on ground, underground, and elevated. Designing these tanks requires attention not only upon strength requirements, but also durability and crack control to prevent corrosion of the steel reinforcement embedded in concrete. The corrosion of steel rebars in reinforced concrete structures (RCS) such as water tanks has become a serious issue and it is considered one of the most significant durability problems of RC elements owing to the danger of failure (Choi et al. 2014; Fang et al. 2017; Ji et al. 2015; Patil et al. 2014). Owing to the heterogeneity of concrete cover and the randomness of external environments, steel rebars in RC members have different degrees of corrosion (Zhao and Fu 2018). Consequently, the corrosion rate and condition of the steel rebars are difficult to evaluate.

On the other hand, the costs due to corrosion can hardly be overestimated. It has been reported that, in the United States alone, the total corrosion-related costs in 2012 amounted to above $1 trillion, no less than 6.2% of the gross domestic product (GDP) (Ishii and Boyer 2011; Jazdzewska et al. 2016). According to the American Water Works Association, the costs due to corrosion of drinking water and sewer systems make up 75% of annual corrosion costs (Mohamed and Benmokrane 2014). The penetration of harmful elements, such as sulfate ions, chloride ions, and atmospheric carbon dioxide, into a highly permeable medium such as concrete has serious impacts on the serviceability of RCS (Pradhan 2014).

Steel rebars in RC members are normally in a passive state owing to a very thin, dense, and stable iron oxide film called the passive layer. This film plays an important role in the protection of steel rebars from corrosion by reducing ions. As a result of this exposure, elimination of the passive film takes place, in which the passive state of the steel rebars changes into an active state. Thus, the corrosion rate can increase drastically because of the degradation of the passive layer. The corrosion of steel rebars in concrete begins when the chloride content at the rebar's surface exceeds a critical value (Brenna et al. 2017) or the penetration of carbon dioxide from the atmosphere through concrete pores decreases the alkalinity of the pore's solution (Berrocal et al. 2016).

[1]M.Sc. Student, Dept. of Metallurgical and Materials Engineering, Faculty of Engineering, Ferdowsi Univ. of Mashhad, Mashhad 91775-1111, Iran. ORCID: https://orcid.org/0000-0003-2014-1057. Email: imantaji@um.ac.ir

[2]Ph.D. Student, Magnel-Vandepitte Laboratory, Dept. of Structural Engineering and Building Materials, Faculty of Engineering and Architecture, Ghent Univ., Tech Lane Ghent Science Park, Campus A, Technologiepark Zwijnaarde 60, B-9052 Gent, Belgium. Email: Saeid.ghorbani@ugent.be

[3]M.Sc. Student, Dept. of Metallurgical and Materials Engineering, Faculty of Engineering, Ferdowsi Univ. of Mashhad, Mashhad 91775-1111, Iran. Email: Johary.reza@gmail.com

[4]M.Sc. Student, Dept. of Metallurgical and Materials Engineering, Faculty of Engineering, Ferdowsi Univ. of Mashhad, Mashhad 91775-1111, Iran. Email: mehrdad.zhp@gmail.com

[5]Associate Professor, Dept. of Metallurgical and Materials Engineering, Faculty of Engineering, Ferdowsi Univ. of Mashhad, Mashhad 91775-1111, Iran. Email: a.davodi@um.ac.ir

[6]Research Engineer, Tousab Consulting and Engineering Company, Payam St., Mashhad 91775-1569, Iran. Email: arashrshebani@gmail.com

[7]Research Engineer, Mashhad Water and Waste Water Company, Ershad St., Mashhad 91735-1139, Iran. Email: mohammadrezamohammadi.abfa@gmail.com

[8]Professor, Dept. of Civil Engineering, Architecture and Georresources, Instituto Superior Técnico, Universidade de Lisboa, Lisbon 1042-001, Portugal (corresponding author). Email: jb@civil.ist.utl.pt

Note. This manuscript was submitted on April 10, 2019; approved on March 5, 2020; published online on May 26, 2020. Discussion period open until October 26, 2020; separate discussions must be submitted for individual papers. This paper is part of the ***Journal of Performance of Constructed Facilities***, © ASCE, ISSN 0887-3828.

This corrosion process is affected by several factors, such as carbon dioxide content, chloride content, concrete diffusion properties, concrete pH value, chemical composition of the steel rebar, existence of voids in the steel rebar/concrete interface, and electrochemical potential of the steel rebar surface (Brenna et al. 2017). The corrosion properties of steel rebars in RCS greatly affect their mechanical performance, durability evolution, and in-service reliability. Therefore, monitoring programs are mandatory to evaluate the different characteristics of the steel rebars in RCS. A monitoring program may be carried out by controlled laboratory studies or field experiments or a combination of both. Field experiments for evaluation of the durability properties of steel rebars in RCS require a long period of time and a huge amount of effort because of the specificity of the steel rebars' corrosion. Therefore, laboratory tests have been developed to shorten the experimental cycle. Laboratory studies mostly take the form of electrochemical impedance spectroscopy (EIS), open circuit potential (OCP), linear polarization resistance (LPR), and Tafel polarization (Flitt and Schweinsberg 2005; Mansfeld 2005; McCafferty 2005). These tests can be used to assess the corrosion resistance of steel rebars in RCS and estimate their service life in a short period of time (Liu et al. 2016).

Corrosion of the steel rebars in RCS, such as water tanks, is considered one of the most significant durability problems of RC elements. Because there is also lack of information about the corrosion performance of RCS after a long period of serviceability (more than 50 years), the purpose of this study is to evaluate the corrosion degree, corrosion rate, durability, and serviceability of steel rebars in a reinforced concrete tap water-storage tank in Mashhad city after a period of 65 years in service. For this purpose, a set of electrochemical tests, including OCP, EIS, and chloride permeability, were conducted on 27 cylindrical concrete cores from different locations on the water tank.

## Description of the Case Study

The Koohsangi's tank was designed by German engineers in the southeast of Mashhad city. It was built between 1952 and 1954, with a cylindrical shape with a diameter of 52 m and a height of 8.5 m. The tank's storage volume is about 15,000 $m^3$. Owing to the pitch of the structure floor, the perimeter walls of the tank have a height of 7.5 m. The ceiling of the structure is connected to the floor by 30 × 30-cm columns aligned in four rows. The structural plan and cross section of the tank are schematically shown in Fig. 1. The roof of the structure is a continuous slab with a thickness of 40 cm and two rows of reinforcement meshes. To determine the compressive strength of the concrete specimens and the yield strength of the reinforcement, several cores were drilled out from different locations on the water-storage tank. An average of 10

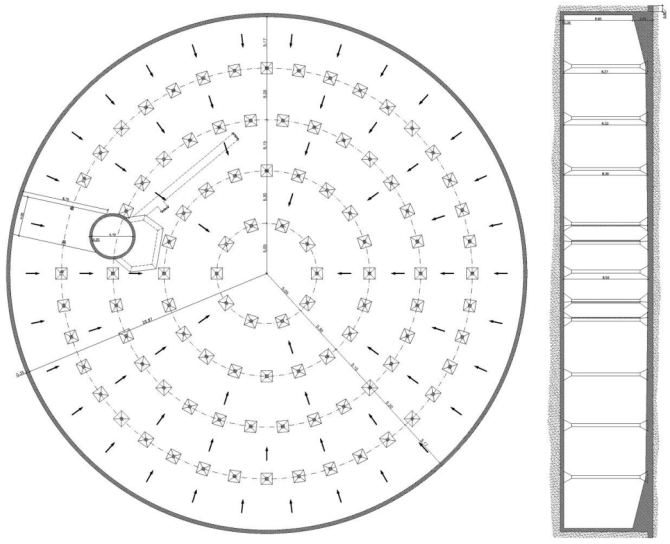

**Fig. 1.** Structural plan and cross section of the underground water-storage tank.

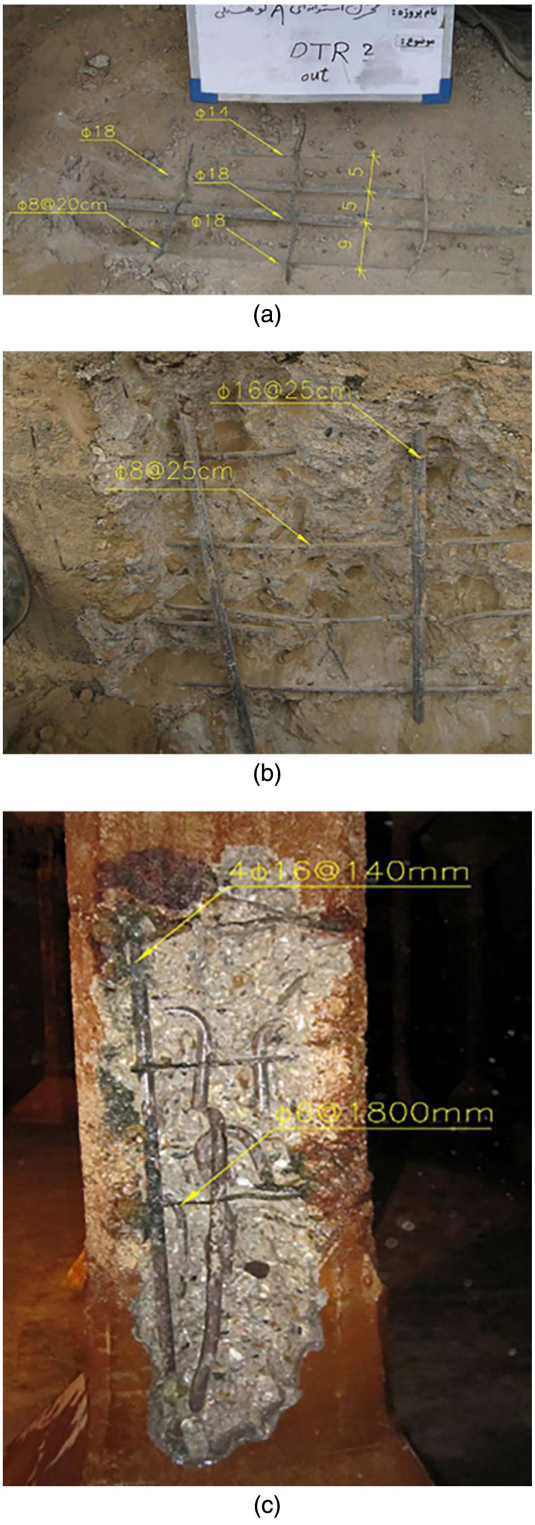


**Fig. 2.** Steel rebar configuration of the tank's: (a) ceiling; (b) perimeter walls; and (c) columns. (Images by authors.)

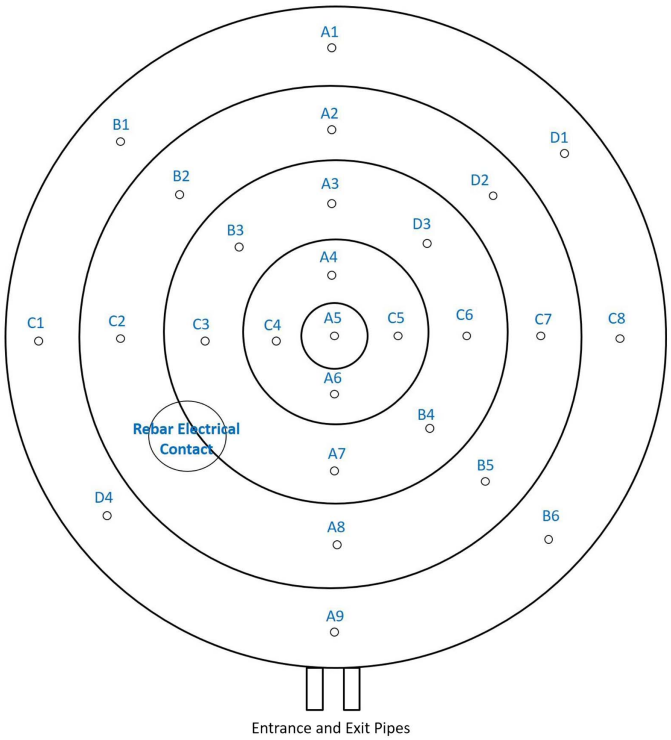


**Fig. 3.** Location of the drilled cores.

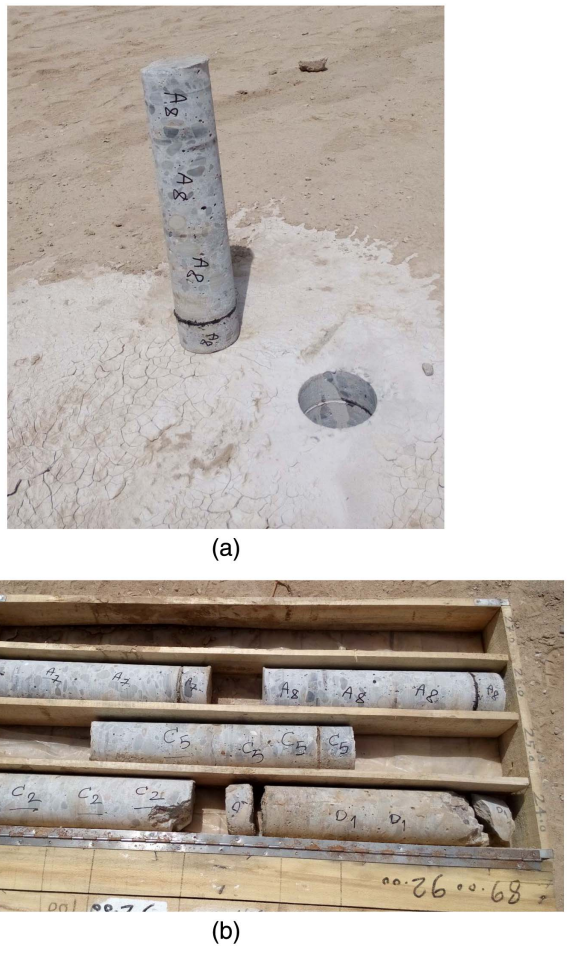


**Fig. 4.** (a) Typical cylindrical core; and (b) delivery box of the cylindrical cores. (Images by authors.)

Schmidt hammer hits was used to measure the rebound of the specimens to determine the concrete specimens' compressive strength. The minimum yield strength of the reinforcements was determined according ASTM A370 (ASTM 2019). The compressive strength of the concrete mix and the minimum yield strength of the reinforcement were about 38 and 285 MPa, respectively. The structure's roof was covered with soil 50 cm thick for aesthetic reasons. Fig. 2 shows the steel rebar configuration of the structure's roof, perimeter walls, and column areas.

## Experimental Procedure

To determine the corrosion performance (steel rebars) of the tank, a preliminary visual survey of the structure was carried out both from the ground and underground, to assess visible signs of damage. Afterward, to inspect and evaluate the corrosion performance (corrosion degree, corrosion rate, and serviceability) of the steel rebars, 27 locations on the roof were selected and cylindrical cores (with diameter of 15 cm) were drilled out and delivered in boxes open to the air for further laboratory investigations. These investigations were performed one day after the drilling process. Locations of the cores were chosen to be a reasonable representation of the entire roof surface. Locations of the cores are shown in Fig. 3. Then, the cores (Fig. 4) were sent to the laboratory for further investigation.

The corrosion behavior of the steel rebars was studied by measuring half-cell potential, EIS, and chloride permeability. The corrosion potential or half-cell potential tests were carried out according to ASTM C876 (ASTM 2015). A direct electrical connection to the steel rebar was used to connect the positive terminal of the voltmeter. Before connecting, the rebar surface was cleaned with a wire brush until the surface shone, to ensure a low resistance connection. The locations subjected to the potential measurement were premoistened and then the potential was measured with a copper–copper sulfate (CCS) reference electrode attached to the concrete surface. All the OCP measurements were carried out inside the holes of the drilled part, so the concrete cover had no effect on the measurements (Elsener et al. 2003).

Chloride permeability measurements were conducted on the cylindrical cores at different depths through the thickness of the roof to obtain the chloride content that had diffused into the roof of the tank. In this regard, depths of 1, 4, 7, 12, 22, and 40 cm from the bottom of the cores were selected, as seen in Fig. 5. Because chloride ions penetrated from the bottom of the roof, smaller increments of depth were selected near the bottom of the cylindrical cores. Afterward, to determine the chloride permeability of the cores, about 20 g of the specimens were collected in the form of powder from the selected spots using a rotatory impact drill. Because the aim of the procedure was to evaluate the concentration of chloride ions in cement, careful attention was paid in order not to drill the aggregates. The chloride was extracted from the collected powder in the solution using hot water and then treated with nitric acid and hydrogen peroxide according to ASTM C1218 (ASTM 2017). Then, potentiometric titration with silver nitrate was used to measure the chloride content of the powder based on ASTM C114 (ASTM 2018).

EIS was carried out on the steel rebars that remained in the drilled cylindrical specimens. The EIS amplitude was 10 mV and it was conducted with a Zive Lab potentiostat (WonATech, Seoul) at a frequency of 100,000–0.1 Hz. The reference electrode was a saturated calomel electrode (SCE) and a platinum wire was used as a counter electrode. Core number A5, which was extracted from the center of the water tank's roof, was selected to evaluate the



J. Perform. Constr. Facil., 2020, 34(4): 04020077

corrosion rate of the different rows of steel rebars. To conduct a test, electrical contact was established by welding a copper wire to the surface of the steel rebar emerging from the core's surface. Afterward, the surface was covered with insulating wax to ensure that it would not be in direct contact with the water. Then, the core was immersed in 3.5% by weight NaCl solution. The setup is shown schematically in Fig. 6.

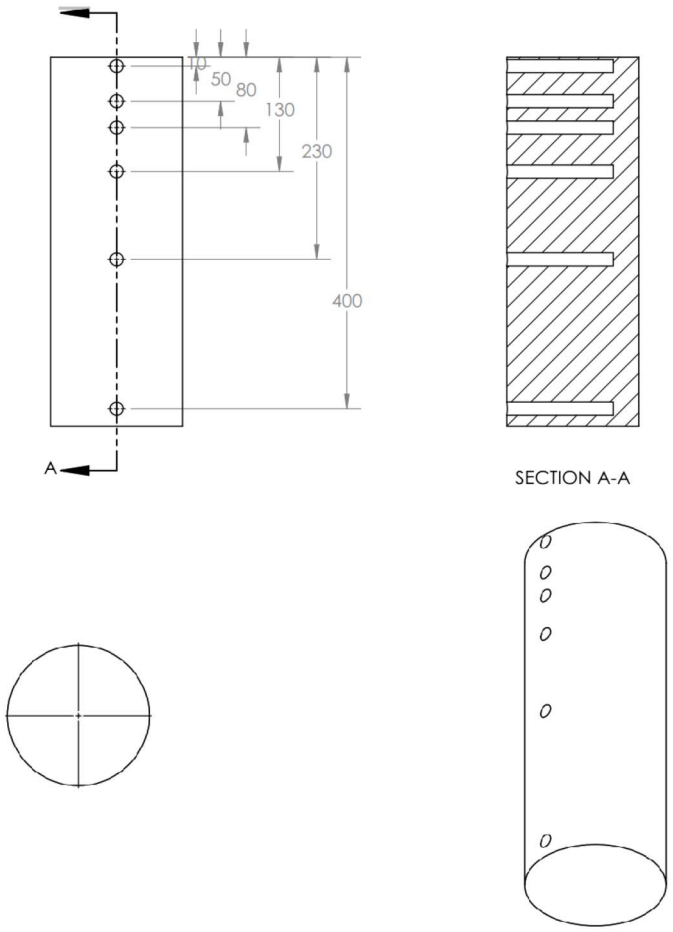


**Fig. 5.** Depths of a drilled core to obtain powder and evaluate the chloride penetration content. The depths are in millimeters from the bottom of the tank's roof.

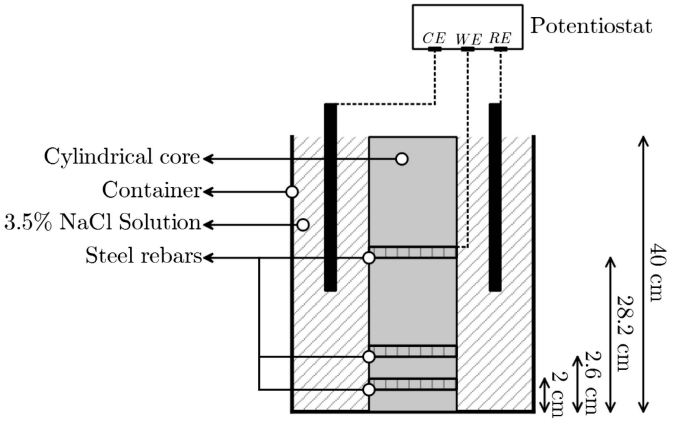


**Fig. 6.** Schematic diagram of the EIS setup used to measure the corrosion rate of steel rebars embedded in concrete at different distances from the bottom of the drilled core.

## Result and Discussion

### Visual Inspections

There is no ventilator to extract the humidity and chloride-laden vapor from the tank. The overflow room, which is the only possible way to exhaust the humidity and chloride vapor, had been sealed for several years. Therefore, the relative humidity in the tank was measured at 90%. The high humidity and lack of exhaust of the chloride vapor made the structure of the tank vulnerable to corrosion damage. Red stains were observed in almost the entire inside surface of the roof. The concrete cover, which was reported to be 4 cm, fell short in many places and corroded steel rebars appeared clearly [Fig. 7(a)]. The piping system was also severely corroded, as seen in Fig. 7(b). Because of the ingress of corrosion products into the concrete and their volume expansion, many cracks were also observed on the roof from the inside (concrete cover) of the tank.

### Corrosion Potential

Measuring OCP or half-cell potential as described in ASTM C876 is the simplest preliminary electrochemical experiment to evaluate the corrosion state of steel rebars in RC members (Trejo et al. 2009). The electrical contact of the steel rebar connected via the tank's overflow room is shown in Fig. 3. Careful attention was paid to the length of the electrical wires to meet the specifications of ASTM C876. All measurements were carried out inside the holes of the drilled cores at the same height of the building structure. Fig. 8 represents the contour diagram of the measured potentials. As seen in Fig. 8, the distribution of the potentials varies between −190 and −250 mV/CCS, which means that almost all the steel rebars were in the area of uncertain corrosion, according to ASTM C876. In this region (where the potential varies from −200 to −350 mV/CCS),

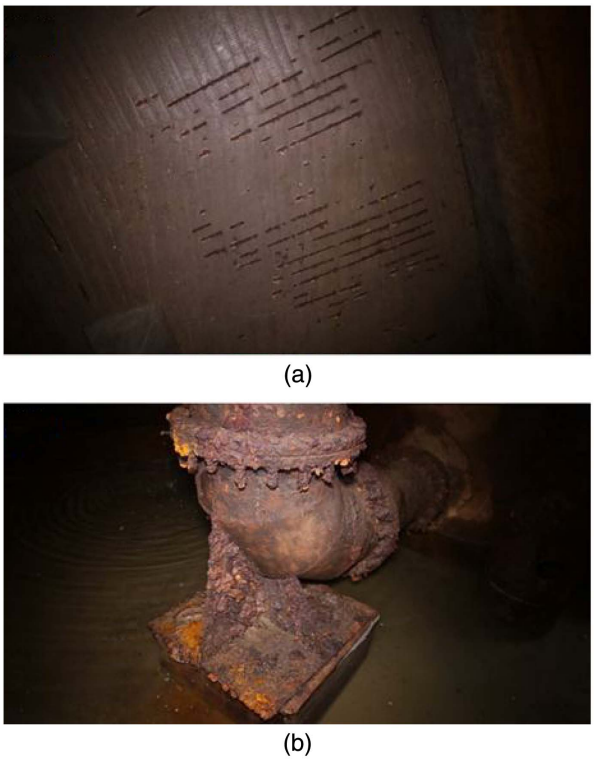


**Fig. 7.** (a) Concrete cover removed exposing corroded steel rebars at the roof surface of the reservoir; and (b) severe corrosion in the pipeline system. (Images by authors.)

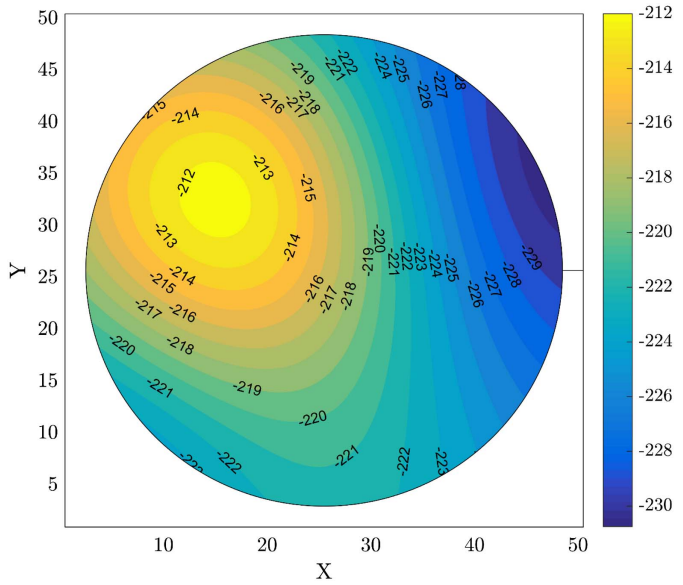


**Fig. 8.** Potential distribution of the tank's roof measured from the outside with reference to a copper–copper sulfate electrode.

the corrosion state of the steel rebars was unknown and further investigations were needed to clarify the exact corrosion behavior of the tank's structure.

Regarding the results of the corrosion potential, two hints should be kept in mind. First, and generally, the OCP measurements in RC structures do not provide any information about the rate of the steel rebars' corrosion. They can only be used to identify whether the steel rebar is in dangerous or safe condition as far as corrosion damage is considered. Therefore, it is better to use this method with other monitoring methods such as EIS to better interpret the results. Second, in this case, corrosion of the steel rebars mostly occurs at the bottom parts of the roof, which are in direct contact with the moisture and chloride vapor. Hence, the upper rows of the steel rebars were not significantly affected. In this structure, all the steel rebar rows embedded in concrete are electrically contacted and subsequently the corrosion potential obtained for each spot is the overall potential of underlying damaged and upper undamaged steel rebars. If it were possible to electrically disconnect the steel rebar rows, more negative potentials might be obtained in the lower rows and more positive ones in the upper rows. The difference in corrosion rates between the lower and upper steel rebar rows will be shown in the EIS section and was obtained by measuring the corrosion rate of the separated rows in drilled parts. As a result, OCP measurements show that the structure is generally not in danger due to corrosion of the steel rebars. However, special attention should be paid to the bottom parts of the roof.

### *Chloride Permeability*

The chlorine content in the water stored in the water-storage tank varies and depends on the seasonal changes and special refining processes, but it is usually kept roughly between 0.55 and 0.65 ppm. Because chloride is the main chemical agent for water treatment in this system, it can be considered the main cause of the steel rebars' corrosion in the tank's structure. Therefore, measuring the chloride penetration into the concrete's depth is necessary to evaluate the corrosion state of the steel rebars. In this regard, the chloride content at different distances from the bottom of the cylindrical cores was measured according to the standard test used to determine the chloride content. All measurement results can be found in Table 1. The contour distribution of the chloride at different distances from the inside surface of the roof is shown in Fig. 9; as the distance from the lower part of the roof increases, the content of chloride ions decreases. At a depth of 1 cm, the content distribution varies between 0.06% and 0.14% by weight, while at 40 cm it varies between 0.035% and 0.08% by weight. At nearly all depths, the furthest location from the entrance and exit pipes had the lowest amount of chloride content, as shown in Fig. 3. It seems reasonable that a greater flow of water containing chloride near the entrance and exit pipes can result in greater evaporation and hence greater content of chloride diffusion into the roof of the water-storage tank in these areas. However, at the opposite part of the structure, where the water is more stagnant, evaporation was lower, leading to less chloride penetration into the roof structure. In addition, based on Fig. 9, it is clear that the chloride content on the left-hand side of the structure is more than that of the right-hand side. This phenomenon can be attributed to the confined area that has formed behind the overflow room, which makes the water vapor, containing chloride, accumulate near the roof structure of the water-storage tank in this area. Additionally, considering the depths of 7, 12, and 22 cm in Fig. 9, it can be inferred that there is little difference in the chloride content on the right-hand side of the structure, while greater differences can be observed in terms of chloride content on the left-hand side. Such differences can be explained by taking into account the diffusion process in the structure. The chloride content at various depths over time can be expressed by the well-known Fick's law:

$$\frac{\partial c}{\partial t} = D\frac{\partial^2 c}{\partial x^2} \tag{1}$$

where $c$ = chloride concentration with diffused depth of $x$ at moment $t$; and $D$ = diffusion coefficient. Based on this equation, one can say that the diffusion of the chloride inside the roof of the water-storage tank is mainly a function of the diffusion coefficient, time, and surface concentration of the chloride. Assuming that the diffusion coefficient and time were the same for the right- and left-hand sides, the difference in surface concentration of the chloride could be the reason for the different diffusion profile of these two sides. On the left-hand side, because of the confined area mentioned previously, the surface concentration of chloride is higher than in the other areas; therefore, a higher variation in the diffusion profile is expected.

There are several references regarding the determination of the chloride threshold of concrete (Trejo et al. 2009; Ann and Song 2007; Oh et al. 2003; Ribeiro and Abrantes 2016). Actually, this threshold can vary according to cement type, mix composition, water content, and temperature, among other factors. However, there are rough estimates that indicate the threshold value. This value can be defined as the content of chloride that is necessary to sustain local passive film breakdown of the steel rebar and hence initiate the corrosion process (Ann and Song 2007). The American Concrete Institute [ACI 201 (ACI 2008)] proposed a threshold chloride content of 0.1% by weight RCS exposed to chloride in service. Oh et al. (2003) also noted that a value of 0.1% by weight can be a good approximation of the threshold concentration of the chloride. Relative to this threshold, nearly 50% of the tank's structure at the depth of 1 cm exceeds the critical value. The chloride content decreases as the distance from the bottom of the roof increases. At 12 cm, only the left-hand side of the water-storage tank roof was under the risk of corrosion damage. Fig. 8 shows that at 22 cm, the highest concentration of chloride content does not reach the 0.1% by weight threshold value.

**Table 1.** Detailed results of the chloride concentration and half-cell potential measurements

| Rod sample | Coordination of drilled core (m)[a] | | Weight percentage chloride to cement concentration | | | | | | | Potential (mV/CCS) |
|---|---|---|---|---|---|---|---|---|---|---|
| | | | Depth from the bottom of the roof (cm) | | | | | | | |
| | X | Y | 1 | 4 | 7 | 12 | 22 | 35 | 40 | |
| A1 | 26 | 48.5 | 0.05 | 0.046 | 0.041 | 0.04 | 0.038 | 0.023 | — | −234 |
| A2 | 26 | 42.5 | 0.038 | 0.036 | 0.034 | 0.03 | 0.03 | — | 0.028 | −209 |
| A3 | 26 | 36.5 | 0.08 | 0.076 | 0.072 | 0.048 | 0.046 | 0.04 | — | −225 |
| A4 | 26 | 31 | —[b] | — | 0.062 | 0.06 | 0.054 | — | 0.042 | −238 |
| A5 | 26 | 26 | 0.084 | 0.08 | 0.065 | 0.05 | 0.043 | 0.038 | — | −215 |
| A6 | 26 | 21 | — | — | — | — | 0.082 | — | 0.076 | −223 |
| A7 | 26 | 15.5 | 0.096 | 0.084 | 0.078 | 0.052 | 0.048 | 0.042 | — | −212 |
| A8 | 26 | 10 | 0.082 | 0.08 | 0.076 | 0.072 | 0.068 | 0.056 | — | −221 |
| A9 | 26 | 3 | 0.11 | 0.1 | 0.091 | | 0.09 | — | 0.078 | −215 |
| B1 | 11 | 44 | 0.16 | 0.15 | 0.14 | 0.12 | 0.11 | 0.1 | — | −227 |
| B2 | 15 | 39 | 0.084 | 0.078 | 0.07 | 0.068 | 0.056 | 0.038 | — | −189 |
| B3 | 19 | 33.5 | 0.06 | 0.045 | 0.04 | 0.032 | 0.03 | 0.03 | — | −190 |
| B4 | 33.5 | 18.5 | 0.1 | 0.09 | 0.09 | 0.09 | 0.082 | 0.08 | — | −235 |
| B5 | 37.5 | 14.5 | 0.07 | 0.066 | 0.052 | 0.047 | 0.042 | 0.04 | — | −212 |
| B6 | 42.5 | 10 | 0.15 | 0.14 | 0.13 | 0.1 | 0.1 | — | 0.05 | −233 |
| C1 | 2.5 | 26 | — | — | 0.17 | 0.16 | 0.12 | 0.08 | — | −219 |
| C2 | 9 | 26 | 0.15 | 0.15 | 0.13 | 0.097 | 0.085 | 0.073 | — | −212 |
| C3 | 15.5 | 26 | 0.099 | 0.083 | 0.066 | 0.052 | 0.043 | 0.039 | — | −200 |
| C4 | 21.5 | 26 | 0.069 | 0.061 | 0.05 | | 0.043 | 0.041 | — | −211 |
| C5 | 31 | 26 | 0.078 | 0.076 | 0.065 | 0.051 | 0.046 | — | 0.043 | −207 |
| C6 | 36.5 | 26 | — | — | 0.067 | 0.055 | 0.041 | 0.039 | — | −227 |
| C7 | 42 | 26 | 0.08 | — | — | — | — | — | — | −219 |
| C8 | 48.5 | 26 | 0.074 | 0.071 | — | — | — | — | — | −244 |
| D1 | 44 | 40 | 0.082 | — | — | 0.063 | 0.055 | — | 0.039 | −237 |
| D2 | 38.5 | 37 | 0.074 | 0.069 | 0.063 | 0.056 | 0.051 | — | 0.042 | −219 |
| D3 | 33 | 33.5 | 0.071 | — | 0.065 | 0.058 | 0.042 | — | 0.04 | −221 |
| D4 | 8 | 12 | 0.14 | 0.12 | | 0.09 | 0.081 | — | 0.075 | −250 |

[a]The locations of the drilled spots on the roof surface are depicted in Fig. 3.
[b]Dashes indicate that the measurement was not possible owing to interference of aggregates.

### *Electrochemical Impedance Spectroscopy*

As stated in the OCP measurement analysis, no urgent corrosion risk can be detected by this technique. However, visual inspections showed clear corrosion damage in the inner parts of the roof. Therefore, differentiation between the corrosion rates of the steel rebars at different depths is necessary to understand the corrosion damage of the structure. Thus, accelerated EIS measurements were carried out to evaluate the corrosion status of the steel rebar embedded in cylindrical cores. EIS is a powerful technique to characterize a wide variety of electrochemical systems and to detect small corrosion occurrences in metallic parts (Ghorbani et al. 2018; Ribeiro and Abrantes 2016; Taji et al. 2019). It is also a common technique and tool to evaluate and study corrosion in RC members (Ghorbani et al. 2018, 2019). Table 2 shows the results of the impedance measurements in the A5 sample located in the middle of the tank's roof at three different distances from the bottom of the roof. The value $R_t$ represents the charge transfer corrosion resistance obtained by fitting the Nyquest diagrams by common equivalent electrical circuit for embedded concrete structures (Ghorbani et al. 2018). The value $i_{corr}$ denotes the corrosion rate of the electrodes in $mA/cm^2$ calculated from $R_t$ data using the Stern–Geary equation and assuming the $B$ constant value equals 52 (Mansfeld 1976). Finally, the corrosion rate in mm/year was calculated using Faraday's law as follows:

$$W = \frac{ItA}{nF} \tag{2}$$

where $W$ = mass of the corroded metal; $I$ = current density in amperes; $t$ = time in seconds; $A$ = atomic weight of steel; $n$ = number of equivalents transferred per mole of metal (assuming 2 for steel); and $F$ = Faraday's constant. Then, the reduction of diameter in a steel rebar per year can be calculated using the density and molar mass of the metal. The resulting values are listed in Table 2. Visual observation of the corroded rebars showed that in most cases the diameter of the rebars that was exposed to corrosion decreased by about 1–2 mm. Based on the corrosion rate measured by the EIS technique 2 cm from the bottom of the tank's roof, it takes about 3–6 years to reach such a level of diameter reduction. However, it should be noted that the corrosion rate reported by the EIS technique represents only the current corrosion rate of the steel rebars. Therefore, it is expected that such corrosion development takes longer than this to occur.

As seen in Table 1, the corrosion rate decreases as the distance from the bottom of the roof increases. According to Alonso et al. (2000), active corrosion in RC structures usually occurs when, in a small exposed area, the corrosion rate of the steel rebar is higher than 0.1 $\mu A/cm^2$. However, Mohammed and Hamada (2001) showed that this value is a very conservative threshold for the corrosion rate. González et al. (1995) reported that the pit penetration rate may be up to 10 times higher (1 $\mu A/cm^2$) at the bottom of the pit. Furthermore, it has been reported that, if the corrosion rate exceeds 1 $\mu A/cm^2$, a high corrosion level should be expected (Andrade and Alonso 1996). By considering 1 $\mu A/cm^2$ as the threshold value, it can be inferred that at the distances of 2 and 2.6 cm from the bottom of the roof, corrosion is significant (13 and 8 $\mu A/cm^2$, respectively) and at 28.5 cm the corrosion rate is too low for it to be considered a high-risk area (0.4 $\mu A/cm^2$).

The corrosion of steel rebars can have harmful effects on both the rebar's mechanical properties and the RCS. Reducing the cross-section area of the steel rebar leads to the deterioration of

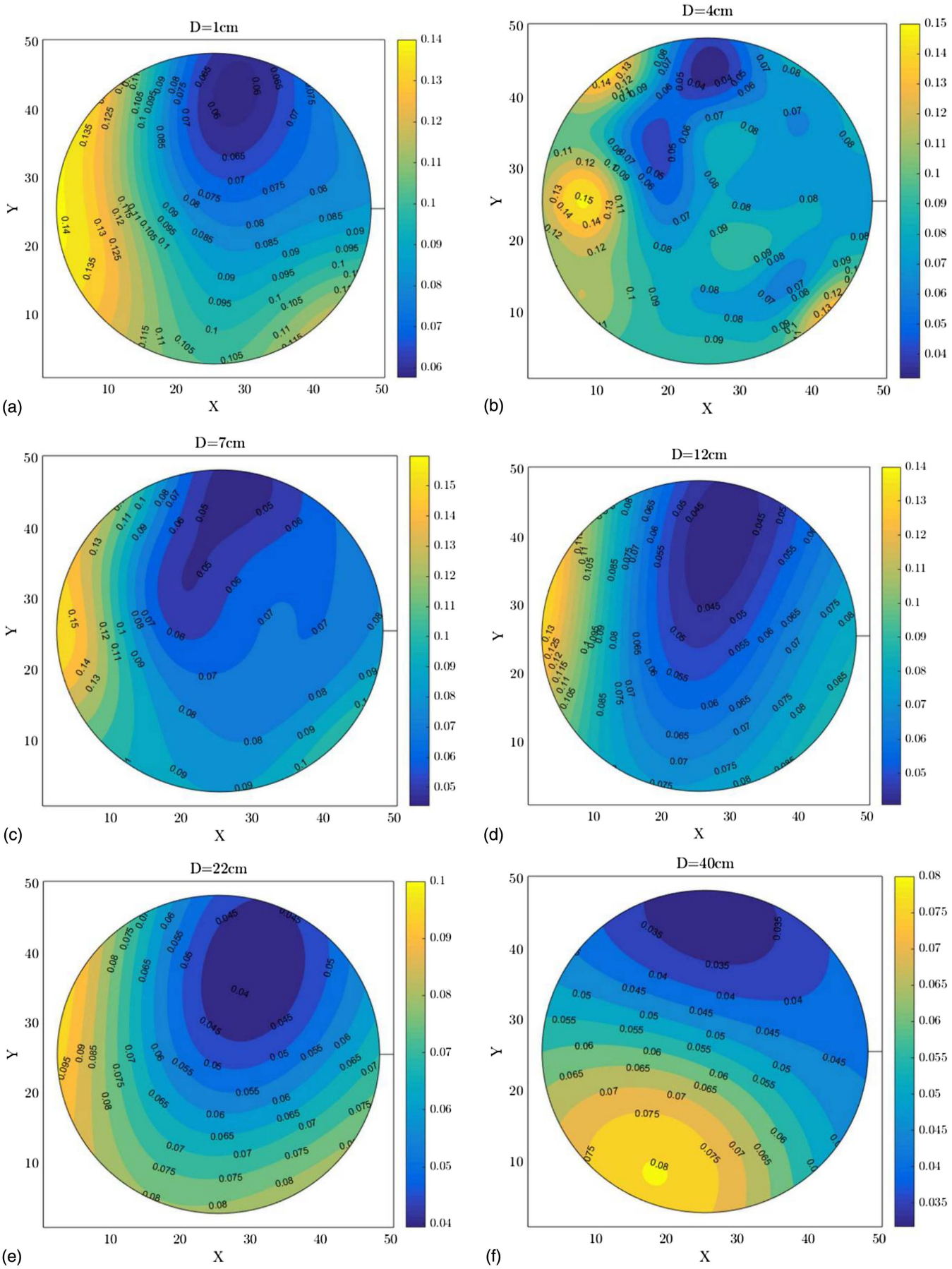


**Fig. 9.** Concentration of chloride by cement weight (%) at different distances from the bottom of the tank's roof.

**Table 2.** Impedance measurements on steel rebars at different depths of core A5

| Distance from the bottom of the tank's roof (cm) | $R_{ct}$ (ohm · cm$^2$) | $i_{corr}$ (mA/cm$^2$) | Corrosion rate (mm/year) |
|---|---|---|---|
| 2 | 4,000 | 0.0130 | 0.1508 |
| 2.6 | 6,500 | 0.0080 | 0.0928 |
| 28.5 | 120,000 | 0.0004 | 0.0046 |

mechanical properties such as strength and ductility (Cairns et al. 2005). It can also have strong effects on the adhesion of the steel rebars to concrete. In addition, rust products, which have a larger volume than the original steel, create splitting stresses acting on the concrete, leading to cracking and consequently spalling of the concrete cover (Tahershamsi 2016). In conclusion, it can be stated that the bottom part of the roof (at least up to 12 cm) should be repaired as soon as possible because of corrosion damage and an appropriate air-conditioning system should be installed to delay the corrosion damage caused by the chloride vapor.

## Conclusions

In this work, the corrosion status of a tank's roof was evaluated using visual inspection, half-cell potential, chloride penetration, and electrochemical impedance studies. The OCP of the whole structure in different spots shows that the corrosion state is unknown if only the half-cell potential is considered. Chloride penetration measurements showed that, at a depth greater than 12 cm from the bottom of the roof, the chloride content was lower than the threshold critical value of 0.1 % by weight chlorides to cement. EIS results showed that at a depth 2 and 2.6 cm from the bottom of the roof the corrosion rate is too high, while at 28.5 cm it is below the critical values. Therefore, it is recommended that the bottom part of the roof slab should be repaired to at least a depth of 12 cm. Furthermore, to reduce the effect of chloride and humidity, a proper ventilation system should be installed in the tank.

## Data Availability Statement

All data, models, and code generated or used during the study appear in the published article.

## Acknowledgments

This research was partially supported by Mashhad Water and Waste Water Company under research Grant No. 97338119. The support of the Ferdowsi University of Mashhad and Foundation for Science and Technology, Civil Engineering Research and Innovation for Sustainability (CERIS) Research Center, and Instituto Superior Técnico is also acknowledged.

## Supplemental Materials

Table S1 is available online in the ASCE Library (www.ascelibrary.org).

## References

ACI (American Concrete Institute). 2008. *Guide to durable concrete?* ACI 201.2R-08. Farmington Hills, MI: ACI.

Alonso, C., C. Andrade, M. Castellote, and P. Castro. 2000. "Chloride threshold values to depassivate reinforcing bars embedded in a standardized OPC mortar." *Cem. Concr. Res.* 30 (7): 1047–1055. https://doi.org/10.1016/S0008-8846(00)00265-9.

Andrade, C., and C. Alonso. 1996. "Corrosion rate monitoring in the laboratory and on-site." *Constr. Build. Mater.* 10 (5): 315–328. https://doi.org/10.1016/0950-0618(95)00044-5.

Ann, K. Y., and H.-W. Song. 2007. "Chloride threshold level for corrosion of steel in concrete." *Corros. Sci.* 49 (11): 4113–4133. https://doi.org/10.1016/j.corsci.2007.05.007.

ASTM. 2015. *Standard test method for corrosion potentials of uncoated reinforcing steel in concrete*. ASTM C876. West Conshohocken, PA: ASTM International.

ASTM. 2017. *Standard test method for water-soluble chloride in mortar and concrete*. ASTM C1218/C1218M. West Conshohocken, PA: ASTM International.

ASTM. 2018. *Standard test methods for chemical analysis of hydraulic cement*. ASTM C114. West Conshohocken, PA: ASTM International.

ASTM. 2019. *Standard test methods and definitions for mechanical testing of steel products*. ASTM A370-19e1. West Conshohocken, PA: ASTM International.

Berrocal, C. G., K. Lundgren, and I. Löfgren. 2016. "Corrosion of steel bars embedded in fibre reinforced concrete under chloride attack: State of the art." *Cem. Concr. Res.* 80 (Feb): 69–85. https://doi.org/10.1016/j.cemconres.2015.10.006.

Brenna, A., S. Beretta, F. Bolzoni, M. Pedeferri, and M. Ormellese. 2017. "Effects of AC-interference on chloride-induced corrosion of reinforced concrete." *Constr. Build. Mater.* 137 (Apr): 76–84. https://doi.org/10.1016/j.conbuildmat.2017.01.087.

Cairns, J., G. A. Plizzari, Y. Du, D. W. Law, and C. J. A. M. J. Franzoni. 2005. "Mechanical properties of corrosion-damaged reinforcement." *ACI Mater. J.* 102 (4): 256.

Choi, Y. S., S.-T. Yi, M. Y. Kim, W. Y. Jung, and E. I. Yang. 2014. "Effect of corrosion method of the reinforcing bar on bond characteristics in reinforced concrete specimens." *Constr. Build. Mater.* 54 (Mar): 180–189. https://doi.org/10.1016/j.conbuildmat.2013.12.065.

Elsener, B., C. Andrade, J. Gulikers, R. Polder, and M. Raupach. 2003. "Half-cell potential measurements—Potential mapping on reinforced concrete structures." *Mater. Struct.* 36 (7): 461–471. https://doi.org/10.1007/BF02481526.

Fang, S., E. S.-S. Lam, and W.-Y. Wong. 2017. "Using alkali-activated slag ferrocement to strengthen corroded reinforced concrete columns." *Mater. Struct.* 50 (1): 35. https://doi.org/10.1617/s11527-016-0915-4.

Flitt, H. J., and D. P. Schweinsberg. 2005. "Evaluation of corrosion rate from polarisation curves not exhibiting a Tafel region." *Corros. Sci.* 47 (12): 3034–3052. https://doi.org/10.1016/j.corsci.2005.06.014.

Ghorbani, S., I. Taji, J. de Brito, M. Negahban, S. Ghorbani, M. Tavakkolizadeh, and A. Davoodi. 2019. "Mechanical and durability behaviour of concrete with granite waste dust as partial cement replacement under adverse exposure conditions." *Constr. Build. Mater.* 194 (Jan): 143–152. https://doi.org/10.1016/j.conbuildmat.2018.11.023.

Ghorbani, S., I. Taji, M. Tavakkolizadeh, A. Davoodi, and J. de Brito. 2018. "Improving corrosion resistance of steel rebars in concrete with marble and granite waste dust as partial cement replacement." *Constr. Build. Mater.* 185 (Oct): 110–119. https://doi.org/10.1016/j.conbuildmat.2018.07.066.

González, J. A., C. Andrade, C. Alonso, and S. Feliu. 1995. "Comparison of rates of general corrosion and maximum pitting penetration on concrete embedded steel reinforcement." *Cem. Concr. Res.* 25 (2): 257–264. https://doi.org/10.1016/0008-8846(95)00006-2.

Ishii, S. K., and T. H. Boyer. 2011. "Evaluating the secondary effects of magnetic ion exchange: Focus on corrosion potential in the distribution system." *Desalination* 274 (1–3): 31–38. https://doi.org/10.1016/j.desal.2011.01.061.

Jazdzewska, A., K. Darowicki, J. Orlikowski, S. Krakowiak, K. Zakowski, M. Gruszka, and J. Banas. 2016. "Critical analysis of laboratory measurements and monitoring system of water-pipe network corrosion-case study." *Case Stud. Constr. Mater.* 4 (Jun): 102–107. https://doi.org/10.1016/j.cscm.2016.01.004.

Ji, Y.-S., G. Zhan, Z. Tan, Y. Hu, and F. Gao. 2015. "Process control of reinforcement corrosion in concrete. Part 1: Effect of corrosion products." *Constr. Build. Mater.* 79 (Mar): 214–222. https://doi.org/10.1016/j.conbuildmat.2014.12.083.

Liu, M., X. Cheng, X. Li, J. Hu, Y. Pan, and Z. Jin. 2016. "Indoor accelerated corrosion test and marine field test of corrosion-resistant low-alloy steel rebars." *Case Stud. Constr. Mater.* 5 (Dec): 87–99. https://doi.org/10.1016/j.cscm.2016.09.005.

Mansfeld, F. 1976. "The polarization resistance technique for measuring corrosion currents." In *Advances in corrosion science and technology*, 163–262. Boston: Springer.

Mansfeld, F. 2005. "Tafel slopes and corrosion rates obtained in the pre-Tafel region of polarization curves." *Corros. Sci.* 47 (12): 3178–3186. https://doi.org/10.1016/j.corsci.2005.04.012.

McCafferty, E. 2005. "Validation of corrosion rates measured by the Tafel extrapolation method." *Corros. Sci.* 47 (12): 3202–3215. https://doi.org/10.1016/j.corsci.2005.05.046.

Mohamed, H. M., and B. Benmokrane. 2014. "Design and performance of reinforced concrete water chlorination tank totally reinforced with GFRP bars: Case study." *J. Compos. Constr.* 18 (1): 05013001. https://doi.org/10.1061/(ASCE)CC.1943-5614.0000429.

Mohammed, T. U., and H. Hamada. 2001. "A discussion of the paper 'Chloride threshold values to depassivate reinforcing bars embedded in a standardized OPC mortar' by C. Alonso, C. Andrade, M. Castellote, and P. Castro." *Cem. Concr. Res.* 31 (5): 835–838. https://doi.org/10.1016/S0008-8846(01)00485-9.

Oh, B. H., S. Y. Jang, and Y. Shin. 2003. Experimental investigation of the threshold chloride concentration for corrosion initiation in reinforced concrete structures." *Mag. Concr. Res.* 55 (2): 117–124.

Patil, S., B. Karkare, and S. Goyal. 2014. "Acoustic emission vis-à-vis electrochemical techniques for corrosion monitoring of reinforced concrete element." *Constr. Build. Mater.* 68 (Oct): 326–332. https://doi.org/10.1016/j.conbuildmat.2014.06.068.

Pradhan, B. 2014. "Corrosion behavior of steel reinforcement in concrete exposed to composite chloride–sulfate environment." *Constr. Build. Mater.* 72 (Dec): 398–410. https://doi.org/10.1016/j.conbuildmat.2014.09.026.

Ribeiro, D., and J. Abrantes. 2016. "Application of electrochemical impedance spectroscopy (EIS) to monitor the corrosion of reinforced concrete: A new approach." *Constr. Build. Mater.* 111 (May): 98–104. https://doi.org/10.1016/j.conbuildmat.2016.02.047.

Tahershamsi, M. 2016. *Structural effects of reinforcement corrosion in concrete structures*. Gothenburg, Sweden: Chalmers Univ. of Technology Gothenburg.

Taji, I., S. Ghorbani, J. de Brito, V. W. Y. Tam, S. Sharifi, A. Davoodi, and M. Tavakkolizadeh. 2019. "Application of statistical analysis to evaluate the corrosion resistance of steel rebars embedded in concrete with marble and granite waste dust." *J. Cleaner Prod.* 210 (Feb): 837–846. https://doi.org/10.1016/j.jclepro.2018.11.091.

Trejo, D., C. Halmen, and K. F. Reinschmidt. 2009. *Corrosion performance tests for reinforcing steel in concrete: Technical report*. College Station, TX: Texas Transportation Institute, Texas A&M Univ. System.

Zhao, Z., and L. Fu. 2018. "The probability distribution of pitting for accelerated corrosion reinforcement." *Case Stud. Constr. Mater.* 9 (Dec): e00193. https://doi.org/10.1016/j.cscm.2018.e00193.